PROBABILISTIC TRANSLATIONAL STABILITY OF MULTI-LAYERED COVER SYSTEM BASED ON LIMITED EXPERIMENTAL DATA

Budhaditya Hazra[1], Jishnu Choudhury[2], and Arindam Dey[3*]

[1]Associate Professor, Dept. of Civil Engineering, Indian Institute of Technology Guwahati, Assam 781039, India. Email: budhaditya.hazra@iitg.ac.in

[2]Former P.G. Scholar, Dept. of Civil Engineering, Indian Institute of Technology Guwahati, Assam 781039, India.

[3*]Associate Professor, Dept. of Civil Engineering, and Center for Disaster Management and Research (CDMR), Indian Institute of Technology Guwahati, Assam 781039, India. Email: arindam.dey@iitg.ac.in

[1]

ABSTRACT

Multi-Layered Cover Systems (MLCS) of waste containment facilities are generally prone to translational instabilities, largely governed by their interfacial shear strength parameters. For the reliability assessment of a MLCS, it is necessary to characterize the interfacial shear strength parameters probabilistically. Owing to the uncertainties involved with the sample preparation and subsequent laboratory experimentations, deterministic linear regression based estimates of shear strength parameters becomes an oversimplifying paradigm. Conducting a very large number of repeated experimental trials to estimate shear strength parameters is practically infeasible, and thus geotechnical engineers often resort to best possible inferences from limited data. This necessitates Bayesian regression based approach catering to limited data for layerwise estimates of interfacial shear strength parameters of the MLCS. Informative (Normal) and noninformative priors are utilized

[1]Arindam Dey[3*] is the corresponding author

to get the updated probability distributions of shear strength parameters of the interfaces. These estimates are subsequently adopted to demonstrate reliability assessment of a MLCS system. A novel conceptual paradigm of probabilistic vulnerable interface diagram (PVID) is introduced to identify the most probable vulnerable interfaces of the MLCS when subjected to multiple factors leading to instabilities.

INTRODUCTION

Industrialization and urbanization have led to the growth in radioactive contaminants detrimental to nature (EIA 2014). Near-surface waste disposal facilities (NSDF) comprise multi-layered cover system (MLCS) and multi-layered liners that are made of different soil-geosynthetic composite systems, isolating the low and intermediate-level radioactive waste from the surrounding environment. The configuration of MLCS depends on the type of waste and site conditions (Koerner and Daniel 1997). According to (Koerner and Daniel 1997), the Resource Conservation and Recovery Act (RCRA) subtitle 'C' MLCS configuration is likely to perform better in climatic regions with high rainfall and intense temperatures that prevail in tropical India.

Once the shallow hazardous waste disposal facilities reach their desired storage capacity, MLCSs are constructed to serve the purposes of protection, barrier and separation (Koerner and Daniel 1997). Each interface of a MLCS can be considered a weak shearing-plane susceptible to failure (Koerner and Hwu 1991; Choudhury et al. 2017). It has been highlighted by the researchers that the translational stability of MLCS is critically governed by the interfacial shear-strength, and it is necessary to identify the critical failure interface(s) for affirming the safety of the structure (Mitchell et al. 1990; Yamsani et al. 2016). Formulations have been developed for various scenarios affecting the translational slope stability by incorporating the effects of seepage, seismic forces and characteristic strength of the MLCS components (Koerner and Soong 2005; Xu et al. 2017). Very recently, with the aid of Monte-Carlo simulations, (Soujanya and Basha 2023a) reported a reliability-based stability analysis of the geogrid-reinforced veneer cover system of MSW landfill against sliding failure. Furthermore, (Soujanya and Basha 2023b) also studied the effect of hydrostatic and hydrodynamic pressures on the stability of landfill veneer covers with an internal sleeper.

Importance of interfacial shear characteristics in interpreting the stability of MLCS (Mitchell et al. 1990; Ling and Leschinsky 1997) cannot be overemphasized. Shear strength parameters of the comprising geomaterials (cohesion and internal friction) and the strength parameters of soil–soil or soil–geosynthetic interfaces (adhesion and frictional characteristics) are essential for analysing the stability of a MLCS. Considering the uncertainties associated with these parameters due to various sources (i.e. choice of instrument, measurement errors, sample preparation, the initial density of the material and other unaccounted factors), probabilistic approach becomes imperative in order to obtain the probability distribution of the shear strength parameters. In most of the previous studies, the shear strength parameters have been modeled as uncorrelated normal distributions (Nguyen 1985; Soubra and Mao 2012). Obtaining the experimental parameters of the MLCS system as a whole becomes much more involved when emulated for multiple setups. Under such circumstances, a Bayesian framework for conducting the probabilistic analysis provides an attractive alternative to the conventional frequentist analysis. (Fellin and Oberguggenberger 2012) proposed a Bayesian approach when the sample data size was small (<5) that replaced the confidence intervals by high probability density regions of the posterior distribution. (Wang and Akeju 2016) characterized site-specific joint probability distribution of shear strength parameters and quantified the cross-correlation between them from a limited number of data under the Bayesian framework. (El-Ramly et al. 2002) demonstrated probabilistic analysis of a slope by considering spatial variability of input variables, statistical uncertainty due to limited data, and biases in the adopted empirical factors and correlations. (Griffiths and Fenton 2004) carried out elastoplastic random finite-element slope stability analysis that highlighted the importance of spatial correlation and local averaging on the probability of failure. (Prakash et al. 2021) constructed joint distribution of soil-water characteristic curve (SWCC) parameters using the Bayesian approach and demonstrated its applicability in reliability based design (RBD) of an unsaturated slope. (Ching and Phoon 2019; Wang et al. 2015) have successfully demonstrated the applicability of Bayesian approaches to construct the site-specific distribution of design parameters when there is insufficient data to characterize site-specific variability.

In practice, conventional deterministic analyses are mostly augmented with experiments conducted for a MLCS, obtaining the shear strength parameters of individual geomaterials and the interfaces by fitting linear regression curves. Frequently, such regression lines drawn using two−to−three data points introduce bias in the parameter estimates that may not be sufficient to cater to all the sources of experimental uncertainties, which makes Bayesian regression an attractive alternative (cite). The present work involves Bayesian linear regression based on Hamiltonian Monte Carlo (HMC) algorithm. The key contributions of this paper are: (1) the development of a probabilistic translational stability analysis of MLCS that is barely understood in literature; (2) an analysis based on limited experimental data; and (3) the development of a probabilistic vulnerable interface diagram (PVID) that provides information about the *vehicle movement* induced instability and critical interfaces of the MLCS under the combined influences of slope length, slope inclination and the position of the compacting vehicle.

BACKGROUND

The shear strength parameters can be determined using direct shear and modified direct shear tests [ASTM D3080/3080M, (ASTM 2011)] . Linear regression on the resulting pairs of peak shear stress and the corresponding normal stresses of the sample yields the cohesion and the angle of internal friction at yield state. The linearisation on a specific stress range is expressed by employing Mohr−Coulomb failure criterion (Coulomb 1776; Labuz and Zang 2012). While fitting a linear model, there is an equal probability (5%) for the shear strength parameters to be less than their lower limits and/or more than their upper limits. The standard linear regression, however, has two obstacles. Firstly, when the mean value of cohesion tends to zero, the 5% limit of cohesion may result in negative values, which is a practical impossibility. Secondly, the assumption of Normality of the error is not always true, particularly when the number of datapoints is less (Williams et al. 2013). Furthermore, linear regression on limited data points is prone to noise and overfitting.

The layout of the MLCS and its predefined failure interfaces ($n_i = 1 \ldots n$) are shown in Fig. 1. It is to be noted that all the layers of the MLCS have uniform thickness along their lengths and all of them are equally inclined at an angle β to the horizontal. The procedure specified by (Koerner and Hwu 1991) was adopted by (Yamsani et al. 2019) to obtain the factor of safety (FoS) at the ${n_i}^{th}$ interface as follows:

$$k_1 FoS^2 + k_2 FoS + k_3 = 0 \tag{1}$$

$$k_1 = (W_A - N_A cos\beta) cos\beta \tag{2}$$

$$k_2 = -[(W_A - N_A cos\beta) sin\beta tan\delta_{eq} + (N_A tan\delta + C_a) sin\beta cos\beta + (C + W_P tan\delta_{eq}) sin\beta] \tag{3}$$

$$k_3 = (N_A tan\delta + C_a) sin^2\beta tan\delta_{eq} \tag{4}$$

where, W_A and W_P represents the weights of active and passive wedges; N_A and N_P illustrates the normal forces acting on active and passive wedges; C and C_a are the total cohesive and the adhesive forces. As each of the interfaces have different interfacial friction angles (δ_1, δ_2,.., δ_n), an equivalent interface angle (δ_{eq}) up to ${n_i}^{th}$ interface was proposed by (Yamsani et al. 2019). For evaluating the FoS of the MLCS under the action of a downward moving mini compaction roller (weight W_b = 72 kN, length l_b = 1.2 m, and width w_b = 0.5 m), suitably modified the coefficients k_1, k_2, k_3.

METHODOLOGY: HAMILTONIAN MONTE CARLO BASED BAYESIAN LINEAR REGRESSION

(Yamsani et al. 2016) obtained the shear strength parameters of the selected geomaterials and their interfaces with geosynthetics as highlighted in Table 1 and Table 2, respectively. As the size N of the original set of measured data used by (Yamsani et al. 2016; Yamsani et al. 2019) was small ($N = 3$), standard linear regression loses its credibility as it is prone to noise and overfitting. Thus, the Bayesian Linear Regression approach (Fellin and Oberguggenberger 2012) has been adopted in this study to deal with such a situation.

Consider a random variable X with probability density function $p(\frac{x}{\theta})$, where θ is a vector of statistical parameters and $p(\theta)$ is the prior distribution. For data = $(x_1, x_2, \ldots, x_N)$ given as an independent sample, one can get the posterior distribution $p(\frac{\theta}{data})$ as described in Equation (5).

$$p(\frac{\theta}{data}) = k^{-1} p(\frac{data}{\theta}) p(\theta) \tag{5}$$

$$k = \int p(\frac{data}{\theta}) p(\theta) d\theta \tag{6}$$

$$p(\frac{data}{\theta}) = \prod_{i=1}^{N} p(\frac{x_i}{\theta}) \tag{7}$$

where, k is the normalizing term in the denominator and $p(\frac{data}{\theta})$ is the likelihood function.

The linear model for Mohr-Coulomb's shear strength equation can be described as (Fellin and Oberguggenberger 2012):

$$\tau_f = c + \sigma v + \epsilon \tag{8}$$

where, $v = tan\delta$, c and δ are the shear strength parameters of the interface, and the error term ϵ has zero mean and s_ϵ^2 as variance.

The random variable X is the regressor variable which are the stresses τ_f (shear stress) and σ (normal stress). θ is comprised of regression coefficients c, v. As proposed by (Fellin and Oberguggenberger 2012), the standard deviation s_ϵ can be estimated from the data [Equation (9)].

$$s_\epsilon \approx \frac{q}{\sqrt{N}} \sqrt{\frac{SS_E}{N-2}} \tag{9}$$

where q corresponds to 95%-quantile that can be obtained from Student t-distribution having $(N-2)$ degrees of freedom and SS_E is the residual sum of squares given by Equation (10).

$$SS_E = \sum_{i=1}^{N} (y_i - \hat{y}_i)^2 \tag{10}$$

where, y_i is the observed value and $\hat{y}_i$ is predicted value from linear regression.

In the standard regression model, given σ, the regressor variable τ_f is assumed to be normally distributed with mean $c + \sigma v$ and variance s_ϵ^2 . For a given set of measurement data = (σ_i, τ_{fi}),

$i = 1, 2, 3, \ldots, N$, the likelihood function can be described as Equation (11).

$$p(\frac{data}{\theta}) = (\frac{1}{s_\epsilon\sqrt{2\pi}})^N exp(-\sum_{i=1}^{N}\frac{(\tau_{fi} - c - \sigma_i v)^2}{2s_\epsilon^2}) \tag{11}$$

The limited number of data ($N = 3$) are updated to get samples from the posterior distribution $p(\frac{c,v}{data})$ using both the noninformative and informative priors. Equation (5) has been solved using No-U-Turn-Sampler (NUTS), which is a an extension to HMC algorithm. FoS is determined on these MCMC samples, and a probabilistic vulnerable interface diagram (PVID) for the MLCS has been constructed for both the noninformative and informative cases.

MCMC is an acceptance-rejection sampling algorithm popularly used in Bayesian inference (Gelman et al. 2013). It uses the Markov Chain to reach the target distribution by iteratively correcting the samples from a conventional distribution. It can be mathematically represented as Equation (12).

$$P(X_{j+1} = y | X_j = x_j, X_{j-1} = x_{j-1}, ..., X_0 = x_0) = P(X_{j+1} = y | X_j = x_j) \tag{12}$$

Some of the widely used MCMC algorithms are random-walk Metropolis (Metropolis et al. 1953), Gibbs sampling (Geman and Geman 1984) and NUTS (Hoffman and Gelman 2014). Less efficient random walks have been a drawback for simple methods like the Metropolis algorithm or Gibbs sampling, as it takes a longer duration to converge to the target distribution (Neal 1993). HMC takes care of the random walk approach by transforming the problem into simulating Hamiltonian dynamics (Neal et al. 2011).

The basic idea of HMC is to generate a proposal from a better proposal distribution and improve the acceptance rate by modifying the acceptance part. For the regular MH algorithm, the samples are directly drawn from a proposal density $q(y|x)$. HMC improves this process by incorporating a random momentum vector in the framework of Hamiltonian dynamics. For every position $x \in R^m$ a vector of m elements are required for the momentum. The momentum vector dictates how x moves dynamically in accordance to Hamiltonian Mechanics.

Based on classical mechanics, the Hamiltonian (H) can be defined as:

$$H(\boldsymbol{\theta}, \mathbf{p}) = U(\boldsymbol{\theta}) + K(\mathbf{p}) \tag{13}$$

where $U(\boldsymbol{\theta})$ refers to potential energy and $K(\mathbf{p})$ refers to kinetic energy, respectively, and $\boldsymbol{\theta}$ is a random variable with probability density function $f(\boldsymbol{\theta})$. In the HMC method, an auxiliary momentum variable $\mathbf{p}$ is defined following a normal distribution: $f(\mathbf{p}) \sim N(0, \mathbf{M})$, $\mathbf{M}$ being a covariance matrix. The goal is to obtain samples from the target posterior distribution. The posterior distribution represents our updated knowledge about the parameters (θ) of interest after incorporating observed data. The potential energy function, ($U(\theta)$), is directly related to the negative log-likelihood of the data and the prior distribution on the parameters. Specifically, it refers to negative log posterior space. On the other hand, the density function $f(\theta)$ describes the prior probability distribution of the parameters (θ). It represents our initial beliefs about the parameters before incorporating the observed data.

Sampling is done from the target distribution by picking $\boldsymbol{\theta}$ from joint density $f(\boldsymbol{\theta}, \mathbf{p})$. According to Hamiltonian dynamics, Hamilton's equation describing the movement of samples are provided by eqs. (14) and (15).

$$\frac{d\theta}{dt} = \frac{\partial H}{\partial p} \tag{14}$$

$$\frac{dp}{dt} = \frac{\partial H}{\partial \theta} \tag{15}$$

where t is the fictitious time.

Leapfrog method is mostly used to find an approximate solution for Hamiltonian dynamics. Considering a small time increment η, one can express a basic Leap-Frog integrator as follows:

$$\begin{aligned}
&\text{For } j = 1, \ldots, L: \\
&p_{t+\eta/2} = p_t - \frac{\eta}{2}\frac{\partial U}{\partial \theta}(\theta_t) \\
&\theta_{t+\eta} = \theta_t + \eta\frac{\partial K}{\partial p}(p_{t+\eta/2}) \\
&p_{t+\eta} = p_{t+\eta/2} - \frac{\eta}{2}\frac{\partial U}{\partial \theta}(\theta_{t+\eta}) \\
&t = t + \eta
\end{aligned} \tag{16}$$

However, HMC requires hand-tuning of the two parameters: step size and integration steps in leapfrog (L), to run a simulated Hamiltonian system. NUTS is one such MCMC algorithm that does not require any hand-tuning at all. It selects an appropriate value for L in each iteration automatically. The leapfrog steps are run such that $\boldsymbol{\theta}*$ approaches $\boldsymbol{\theta}$. It is accomplished by taking the derivative of half the squared distance between the current position $\boldsymbol{\theta}*$ and the initial position $\boldsymbol{\theta}$ [Equation (17)].

$$\frac{\partial Q}{\partial \tau} = \frac{\partial(\boldsymbol{\theta}^* - \boldsymbol{\theta})'(\boldsymbol{\theta}^* - \boldsymbol{\theta})}{\partial \tau 2} = (\boldsymbol{\theta}^* - \boldsymbol{\theta})'p < 0 \tag{17}$$

One may refer to (Nishio and Arakawa 2019) to know the sampling procedure in NUTS. The pseudocode and derivations related to NUTS can be referred to (Hoffman and Gelman 2014). The NUTS (No-U-Turn Sampler) algorithm as implemented in the PyMC3 library was employed in the present work. PyMC3 is a popular probabilistic programming framework that provides tools for Bayesian analysis. The NUTS algorithm, which is part of PyMC3, automatically explores the posterior distribution by iteratively sampling from it. The algorithm incorporates the No-U-Turn criterion to determine when to stop sampling, ensuring efficient exploration of the posterior. The algorithms can be sourced to the following website: https://www.pymc.io/projects/docs/en/v5.6.1/learn/core_notebooks/pymc_overview.html

UNIVARIATE PROBABILITY MODELS

In the present study, probability plots have been used to determine the probability distribution. Plots are constructed based on a linear relationship between theoretical quantiles of the candidate probability distribution and the sorted values of the data. In the given study, probability plots for four candidate distributions: Weibull, Normal, Lognormal, and Gumbel are constructed for each interface. The most probable distribution is chosen based on the highest (R^2) value. Filliben (Filliben 1975) provided the estimates to obtain the theoretical quantiles as:

$$m_i = \begin{cases} 1 - 0.5^{1/n} & i = 1 \\ \frac{i-0.3175}{n+0.365} & i = 2, 3, \ldots, n\text{-}1 \\ 0.5^{1/n} & i = n \end{cases} \tag{18}$$

where m_i is the uniform order statistics median. Quantiles are calculated by evaluating percent point function (PPF) at m_i. Here, i is the i^{th} ordered value and n is the total number of values. In PPF, given the probability, the corresponding x for the cumulative distribution function (CDF) is computed.

For the marginal posteriors of interfacial adhesion (c) and $v = tan\delta$ (δ is the interfacial friction angle), the general approach for obtaining the univariate distribution of the posteriors after posterior sampling from the MCMC chain is outlined as follows:

- Sort the values c, v to obtain ordered values.
- Obtain the theoretical quantiles by evaluating PPF of m_i for the assumed candidate distributions.
- For each candidate, plot ordered values versus the theoretical quantiles to get the probability plot and get R^2 value.
- Choose the highest R^2 candidate in the probability plots as the preferred univariate distribution.

NONINFORMATIVE AND INFORMATIVE PRIORS

Noninformative and informative prior knowledge was used to get the updated probability distribution of interface shear properties. The lower limit of c has been kept at 4-6 kPa considering practical scenarios.

Uniformly distributed noninformative priors are chosen on certain intervals as [c_{min}, c_{max}],

$[v_{min}, v_{max}]$. The choice of such priors is advantageous for achieving $c \geq 0$ and $v > 0$ conditions. The choice of c_{max} and v_{max} is such that they are less than the shear strength parameters of the parent materials. However, the geomembrane material referred here is actually a geocomposite comprising layers of geomembrane and geonet sandwiched together, thereby leading to augmented interface shear characteristics that is effectively more than the parent material. The parameters for uniform distribution are the minimum and the maximum value for the random variable. Uniformly distributed priors are expressed as detailed in Equations (19) and (20).

$$p(c) = [c_{max} - c_{min}]^{-1} \tag{19}$$

$$p(v) = [v_{max} - v_{min}]^{-1} \tag{20}$$

For the choice of informative priors, normally distributed priors have been chosen of certain mean and variance. The parameters for normal distribution are the mean and the standard deviation of the random variable. The parameters μ_c, μ_v, σ_c and σ_v of the interfaces are manually adjusted such that $c \geq 0$ and $v > 0$ conditions are satisfied and the bounds mentioned in noninformative prior are not violated. Normally distributed priors are expressed as detailed in Equations (21) and (22).

$$p(c) = \frac{1}{\sigma_c \sqrt{2\pi}} exp^{-\frac{(c-\mu_c)^2}{2\sigma_c^2}} \tag{21}$$

$$p(v) = \frac{1}{\sigma_v \sqrt{2\pi}} exp^{-\frac{(v-\mu_v)^2}{2\sigma_v^2}} \tag{22}$$

Table 3 summarizes the parameters of the uniform and normal priors. These priors are considered based on proper subjective consideration of the interface characteristics.

The choice of the mean and standard deviation of the normal priors for interfacial shear strength properties (c and v) is carefully made, considering the lower and upper limits of the properties obtained from experiments. The means and standard deviations were selected based on the idea that the probabilistically sampled interfacial properties should lie within $(\mu - 3.3\sigma, \mu + 3.3\sigma)$ range, where $(\mu - 3.3\sigma)$ corresponds to lower bound and $(\mu + 3.3\sigma)$ corresponds to the upper bound of the deterministic experimental values. For example, when analysing the interface between Red soil and Geotextile, we considered the specific properties of Red soil, such as its cohesion value of 16.96 kPa, and the measured interfacial adhesion of 13.7 kPa between Red soil and Geotextile. To choose appropriate prior parameters, we set the mean as 10 kPa and the standard deviation as 2 kPa. We used the mean ± 3.3 standard deviations which accounts for approximately 99.99% of the cumulative probability density. This choice ensures that the inferred distribution of interfacial shear strength properties remain well within the bounds of the corresponding interface properties obtained experimentally. This conservative approach ensures that the chosen priors encompass a wider range of possible values, accounting for the inherent uncertainty and variability in the interfacial shear strength properties.

RESULTS AND DISCUSSIONS

For the present study, the data are obtained from laboratory experiments conducted on the selected geomaterials and their corresponding interfaces with the geosythetics (Table 1 and Table 2). For more details the readers are referred elsewhere (Yamsani et al. 2016; Yamsani et al. 2019). The posterior densities of c and v are first obtained using uniform and normal priors that are subsequently utilized for the analyses of the MLCS system.

Effect of Priors

For sampling posteriors from the proposed approach, data points (c,v) with sample size (N = 3) are utilized for analyses. Following the NUTS algorithm, MCMC simulations are performed for the length of the Markov chain ($N_s = 10^4$). The likelihood model being fitted is shown in Equation (11). The parameters for the noninformative priors are the ranges of c and v. The informative priors are normally distributed with parameters and hyperparameters as per Table 3.

For the interface $n_i = 1$, the obtained MCMC samples of size ($N_s = 10^4$) for c and v are presented in Fig. 2. Typical probability plots and the marginal densities of the posteriors for the aforementioned interface are also shown in Fig. 2. R^2 values of the probability plots for each of the candidate posterior distributions are summarized in Table 4.

The R^2 values in Table 4 suggest that Weibull distribution is the best fit distribution for the shear properties of the red soil-geotextile (RS−GT) and geomembrane-bentonite (GM−B) interfaces. In contrast, Normal distribution is the appropriate posterior probability density function for the GT−G, G−S and S−GM interfaces. However, for informative priors, Normal distribution is obtained as the best fit posterior for all the interfaces (Table 4), which corroborates with the analytical Bayesian inference for Gaussian distribution.

Practical Application: Reliability Assessment of MLCS

It is fairly well recognized that experimentally obtained shear strength parameters and interfacial shear parameters are susceptible to uncertainties. One way of overcoming the issue is to perform a large number of repeatable experiments and properly addressing the sampling uncertainties associated with the parameter estimates. However, this approach becomes infeasible due to practical considerations and time consumption. In such cases, perhaps a more rational and practical approach would be to measure the data following the prescribed codal provisions and then use the proposed Bayesian regression framework on limited data. Thus, for the slope stability analysis of the MLCS, the interface parameters of the layers are obtained from the samples of $p(\frac{c,\nu}{data})$ from the estimated posteriors (Equation (5)). The following section illustrates the effect of the noninformative and the informative priors on the translational stability of MLCS incorporating the parametric variations in slope inclination, length of slope, and the effect of a downward moving mini compaction roller.

Reliability of MLCS' stability can be expressed as the probability of failure (P_f) that can be estimated from the limit state function: $g(\mathbf{X}) = \text{FoS} - 1.5$, with the input parameters $\mathbf{X} = (X_1, X_2, ..., X_n) = (H, L, \beta, c, \nu, \phi, \gamma)$. The corresponding probability of failure can be defined as:

$$P_f = P(g(X_1, X_2, ..., X_n) \leq 0) = \int ... \int_{g(\mathbf{X})\leq 0} f_X(x)dx \tag{23}$$

The above can be estimated in the Monte Carlo simulation framework using a standard indicator function as Equation (24).

$$P_f = \frac{1}{N}\sum_{i=1}^{N} I(g(\mathbf{X}) \leq 0) = \frac{1}{N}\sum_{i=1}^{N} I(FoS - 1.5 \leq 0) \tag{24}$$

where, N is the number of observations of FoS, and I is an indicator function for counting the number of times a particular interface of MLCS fails, i.e., FoS≤1.5.

For reliability analysis of MLCS, 10^4 trials of MCS are performed. FoS for an interface of MLCS is given by Equation. (1) and the corresponding P_f can be evaluated by using Equation (24). The application of the proposed approach in developing the probabilistic Vulnerable Interface Diagram (PVID) of the MLCS interfaces is introduced next. This essentially brings out an important concept pertaining to the probabilistic stability of MLCS in relation to the uncertainties involved in the failure of the individual interfaces.

Effect of Slope Inclination

For a surface cover system, (NSWEPA 2015) recommends a mild slope inclination of 3%–7%. However, under certain circumstances, due to the unavailability of sufficient space for facilitating storage of excess waste, slope inclinations as high as 30% have also been reported in the literature (Seed et al. 1990). Accordingly, in the present study, the FoS is evaluated for three different slope inclinations, 10%, 20%, and 30%, which corresponds to slope angles 5.7°, 11.3°, and 16.7° with the horizontal, respectively. In these analyses, the length of the uppermost surface of the MLCS (L) is considered as 30 m.

For brevity, the probability plots obtained after transcribing posterior samples from MCMC into Equation (1) using noninformative (Uniform) and informative (Normal) priors are not presented. R^2 values for each of the candidate distributions are summarized instead, in Table 5. From Table 5, it can be inferred that Normal distribution is the best fit for the FoS samples of all the interfaces and slope inclinations, when Normal priors are considered, although Weibull and Lognormal distribution appears to be equally good candidates. In contrast, when Uniform priors are considered, Weibull distribution appears to be an appropriate PDF for the GM−B interface

(n_i = 5) irrespective of the slope inclination. However, for the remaining interfaces ($n_i = 1 \ldots 4$) the FoS samples of the remaining interfaces are likely to follow Normal distribution for all slope inclinations.

Fig. 3 shows the posterior PDFs of FoS computed at various slope inclinations. For 10% slope, it can be noted that the highest value corresponds approximately to FoS = 6.5, 4.5, 6.1, 5, 8.5 for $n_i = 1, 2, 3, 4, 5$ respectively, regardless of noninformative or informative priors. However, the spread of FoS for the latter case decreases, suggesting that the consideration of Normal priors is more economical from design consideration, yet less conservative from failure perspective. The distribution of FoS is of practical interest as it conforms to one of the most important design checks to be considered while assessing the stability of MLCS. At a relatively gentle slope of 10%, it can be noted that the fraction of FoS≤1.5 is zero, whereas with the increase in β, the fraction of FoS≤1.5 becomes higher, which is an intuitive result.

(Yamsani et al. 2019) identified the GT−G interface ($n_i = 2$) as the critical failure plane, thereby inferring it as the weakest interface. However, a small percentile of the FoS ($X(\zeta) \leq x$; where X is a random variable denoting FoS) falls below the minimum required magnitude of 1.5 for the S−GM interface ($n_i = 4$) at 20% slope inclination indicating it to be unsafe. The interfaces $n_i = 2$ and $n_i = 4$ do not have adhesion, and thus these interfaces would fail for $\delta \leq 8.05°$ and $\delta \leq 12.75°$ respectively, when estimated by satisfying the aforementioned criterion. Furthermore, for a 30% slope, using the same criterion, R−GT interface ($n_i = 1$) and G−S interface ($n_i = 3$) also exhibits failure. Hence, each of the interfaces $n_i = 1 - 4$ would fail for $\delta \leq 13.5°$, $\delta \leq 13.17°$, $\delta \leq 21.42°$ and $\delta \leq 21.53°$ after considering either of the priors for 30% slope inclination. However, the interfacial adhesion values satisfying the aforementioned criterion depend on the choice of priors. In particular, the adhesion (c) for $n_i = 1$ corresponds to $c \leq 16$ kPa and $c \leq 15.04$ kPa, respectively.

Table 6 and 7 summarize the variations of P_f, mean, 95 percentile, and 99 percentile values of FoS with the change in slope inclination and interfaces. It can be noted that P_f increases with the increase in slope inclination. For 10% slope, the P_f is 0 (zero) for all interfaces of the MLCS for both the priors, which is expected from a slope having an inclination ($\approx$ 6°) lesser than the friction angles of all the interfaces of the MLCS (Table 2). On the other hand, the 30% slope is expectedly more susceptible to failure, which is reflected by the mean FoS values much lesser than 1.5 for some interfaces. Given that the angle of slope inclination is (β) $\approx 17°$, $n_i = 2$ with $\delta_i = 9°$ is highly likely to fail ($P_f = 1$). However, the interfaces that have substantial contribution from adhesion as well as interfacial friction are least likely to fail (i.e. $n_i = 5$), whereas, the ones with less $\delta_i < \beta$ as well as relatively lesser cohesion still have a higher likelihood of failure ($n_i = 1$). The system performance in terms of reliability index is still *Hazardous* as per USACE ETL-1110-2-547 (USACE 1997), which is not surprising for a steeper MLCS.

Of significant interest is the MLCS with 20% slope (with inclination $\approx 11°$). Deterministic analysis shows a FoS of all interfaces to be greater than 1.5, thereby signifying sufficiently stable MLCS. However, the proposed Bayesian regression based technique indicates a contrasting result. For $n_i = 2$ and $n_i = 4$, the P_f(s) are 0.15 and 0.055 for Uniform prior, and 0.13 and 0.02 for Normal prior, respectively. Although the probability of failures are still small, as per USACE ETL-1110-2-547 (USACE 1997), the performance level ranges between *Poor* to *Hazardous*. This result underscores the importance of the probabilistic approach for analyzing the translational stability of a MLCS.

Effect of Length

The influence of the length of slope L on the FoS distribution of different interfaces of MLCS is studied for maximum slope inclination (30%).

For the sake of brevity, probability plots for simulated FoS considering uniform and normal priors are not presented here. It is found that the Weibull distribution is the best fit distribution for the FoS samples of interface $n_i = 5$ for L= 15 m, 30 m, 50 m when uniform priors are considered. The Weibull distribution also appears to be the best fit for the FoS samples for interfaces $n_i = 1, 3$ for L = 15 m. The FoS samples for the rest of the interfaces and length conditions follow Normal distribution. The best-fit probability plots correspond to Normal distribution for all the interfaces and length when informative priors are used except for the interfaces $n_i = 4, 5$ for L=15 m. In this case, the best-fit PDF for sampled FoS is the Lognormal distribution.

The FoS distribution obtained from simulated MCMC posterior samples with change in length follows almost similar lines of interpretation as in Fig. 3. At a relatively shorter length of L=15 m, it has been observed that the fraction of FoS <1.5 is less. With the increase in length, the fraction of FoS <1.5 becomes higher.

At L = 50 m, the P_f for $n_i = 1 - 4$ is greater than equal to 0.5 and, in some cases $P_f \approx 1$, indicating that these interfaces are prone to instability for specific c, δ for both the cases of simulations. Although (Yamsani et al. 2019) considered the interface $n_i = 1$ to be safe ($FoS \geq 1.5$) for 30 m length of the slope; however, simulation results considering normal priors show that P_f for these two interfaces is as high as 0.5-0.7. Thus, due consideration also has to be given to interface $n_i = 1$ for stability assessment in addition to the interfaces $n_i = 2, 4$ which has $P_f \approx 1$. In fact, the mean FoS for the interfaces $n_i = 1, 3$ is also on the lower side than the FoS reported by (Yamsani et al. 2019). When the best fit PDF of FoS is Weibull, or, lognormal, for a specific interface, mean FoS will not be an appropriate choice of FoS for the design. In such cases, more conservative values (higher % ile values) will be a better choice for FOS.

Table 8 summarizes the variations of P_f, mean, 95 percentile, and 99 percentile values of FoS with the change in slope length. It can be noted that P_f increases with the increase in the length of slope. For 15 m slope-length, the P_f is 0 (zero) for all interfaces of the MLCS with normal prior, except for S−GM interface which has still hazardous as per as per USACE ETL-1110-2-547 (USACE 1997), which is expected due to the low magnitude of interface friction between sand and geomembrane. For L = 30 and 50 m, the performance level of all the interfaces are Hazardous except for the $n_i = 5$ (i.e. GM-B) which exhibits a poor performance level for the highest slope length considered.

The influence of length on the evaluated FoS is found to be more pronounced for shorter lengths as compared to the longer ones. For the shorter length sections, the driving force responsible for generating the translation movements along each of the interfaces is lower. With increasing lengths, as the driving force gets accumulated, more numbers of interfaces tend to fail. For lesser lengths, component (i.e. interface) failure is more pronounced as opposed to system (i.e. MLCS) failure for higher lengths. Such a trend was reported by (Yamsani et al. 2019) based on the deterministic translational stability analysis of a MLCS. The deterministic FoS reported by (Yamsani et al. 2019) and the mean FoS (in current study) obtained after sampling c, v as posteriors from the MCMC chain ($N_s = 10^4$), with Normal priors are presented in Fig. 4(b) in which all the interfaces show a similar trend.

Effect of Downward Movement of Compacting Vehicle

In this section, the effect of the downward movement of compacting vehicle with constant velocity on the stability of MLCS (30 m length of slope with 30% inclination) has been analyzed in the prescribed probabilistic framework.

It has been found that the Weibull distribution fits best for the FoS samples pertaining to the interface $n_i = 5$ for V = 0 m and the transition point (V represents the height of vehicle above the toe of MLCS) when uniform priors are considered in the simulation. The FoS samples for the rest of the interfaces and vehicle positions in the vertical direction follow Normal distribution. Concurrently, the best-fit probability plots follow Normal distribution for all the interfaces and vehicle positions when informative priors are used. Similarly, for interfaces $n_i = 2 - 5$, lognormal and Normal distribution appears to be the best-fit (R^2-0.999); however, Normal distribution is the preferred distribution for consistency.

As the vehicle traverses from the passive zone to the transition points (from passive to active zones) of each interface, it can be observed from Fig.5 that there is an improvement of FoS. However, the FoS distribution for interface $n_i = 2$ and a portion of FoS distribution for the interfaces $n_i = 1$ and 4 still does not satisfy the FoS >1.5 criterion. The corresponding interfacial shear parameters are c <16 kPa and δ <12.6°, for $n_i = 1$ for uniform priors. When the priors are normal, c <16 kPa and δ <14.81° is likely to cause the failure of interface $n_i = 1$. The failure of interface $n_i = 4$ takes place for δ <14.33° irrespective of the priors considered during the simulation. When the vehicle is located on the active zone (V = 6 m, 12 m), all the interfaces fail to satisfy FoS >1.5 except for $n_i = 5$. There is no change in the FoS distribution for V=6 m and 12 m. (Yamsani et al. 2019) also provided a similar observation. This is attributed to the fact that once the vehicle moves sufficiently away from the transition zone, it ceases to influence the layer wise passive resistance, effectively leading to the same FoS distribution. Further, the interface $n_i = 3$ would remain safe irrespective of the vehicle location on the active zone when $\delta > 23.26°$.

Further from Fig. 5, one can infer that P_f decreases as the vehicle moves from entirely passive zone (V = 0 m) to the transition point (passive to active zone), beyond which it increases approximately to 1 as the vehicle traverses completely into the active zone. The GM-B interface ($n_i = 5$) remains safe for all vehicle positions, irrespective of its location on active or passive zones. For normal prior, it can be observed that P_f =0.717 for $n_i = 1$ when compared to the uniform prior case, where P_f = 0.506 for V = 0 m. Although (Yamsani et al. 2019) considered interface $n_i = 1$ to be safe ($FoS \geq 1.5$) for V = 0 m; however, under the current probabilistic framework considering normal priors, the $n_i = 1$ interface shows a mean $FoS < 1.5$ and $P_f = 0.717$, which pertains a hazardous performance level as per as per USACE ETL-1110-2-547 (USACE 1997).

Fig. 6 presents deterministic FoS reported by (Yamsani et al. 2019) and the Mean FoS with change in vehicle position after sampling c, ν as posteriors from the MCMC chain (N_s=10^4) when the priors are normal. It suggests that the $n_i = 2$ interface is the most critical interface, exhibiting minimal FoS, followed by the interfaces $n_i = 1$ and $n_i = 4$. Further, it is clear that whereas the deterministic study is only able to capture independent interfacial failures (failure of one interface doesn't influence the failure another), the present framework allows identifying more realistic possibilities of correlated failures (failure of one interface influences the failure of another) as the vehicle traverses from active to passive regions across the transition point. This necessitates the development of probabilistic vulnerable interface diagram (PVID) to be illustrated next.

Probabilistic Vulnerable Interface Diagram (PVID)

Probabilistic vulnerable interface diagram (PVID) is developed in this study by combining the FoS distribution of all the interfaces corresponding to different destabilization factors for Normal priors. The diagram helps in identifying the weakest interfaces of a given MLCS configuration, considering all the factors causing instability. As an example, for a MLCS having a slope inclination of 30% and length of 30 m, with the compacting vehicle located near the crown of the slope (i.e., V=12 m above the toe), then the corresponding PVID for the MLCS is depicted in Fig. 7. The left one does not consider any vehicle present on the MLCS. The main objective of this figure is to highlight the two extreme cases involving the presence or absence of vehicle on the MLCS.

For an identical MLCS, (Yamsani et al. 2019) considered both $n_i = 3$ and 5 to be safe according to the deterministic VID, but the PVID (Fig. 7) suggests that a fraction of FoS distribution for $n_i = 3$ also do not satisfy the stability criterion. Accordingly, from the figure, it can be ascertained that only interface $n_i = 5$ qualifies the required FoS subjected to all the factors governing the stability. It can be inferred that the interfaces $n_i = 2$ and $n_i = 4$ are the most vulnerable ones requiring substantial strength improvement.

Comparison with Monte Carlo Simulation

The effect of slope inclination, slope length and the downward movement of the compacting vehicle on the stability of MLCS have also been analyzed using Monte Carlo Simulation (MCS). The statistical parameters mentioned in Table 3 are used to obtain the distributions for c, v. The best-fit probability plots are for the Normal distribution for the sampled FoS irrespective of the slope, length, or vehicle position. The R^2 values of these plots are in the range of 0.9997 to 0.9999. For the sake of brevity, the probability plots are not shown here.

Fig. 8 shows the FoS distribution for the extreme scenarios corresponding to different destabilizing factors considered in this study. It shows that the best-fit distributions are Normal irrespective of interfaces, or, destabilizing factors. However, the general trend for the distributions is more or less similar when compared with simulated FoS from the MCMC cases. The MCMC posteriors are narrower and have sharper peaks, and it is likely that the posteriors obtained from the MCMC simulations considering normal priors are more reliable.

CONCLUSIONS

This study explores the probabilistic estimates of the interfacial shear strength parameters from limited data using Bayesian linear regression. Further, reliability assessment of a MLCS has been carried out by adopting Bayesian linear regression estimates. The following conclusions can be drawn from this study:

- Weibull distribution is appropriate for modeling the interfaces that have both interfacial friction and adhesion, when uniform priors are used. Whereas, Normal distribution is found appropriate for the interfaces devoid of adhesion.
- The Normal distribution is the best fit distribution irrespective of interfacial shear strength parameters when normal priors are used.
- FoS distribution for each interface has been obtained corresponding to various destabilization factors such as slope inclination, length, and the effect of a downward moving compacting vehicle. The fraction of FoS distribution that fails to satisfy the $FoS > 1.5$ criteria is identified from which the corresponding interfacial shear strength parameters are evaluated. This leads to a reliability assessment of the specific MLCS considered in this work.
- Deterministic analysis for 20% slope with 30 m length shows a constant FoS for all interfaces to be greater than 1.5, thereby signifying sufficiently stable MLCS (Yamsani et al. 2019). However, the proposed probabilistic approach shows that for $n_i = 2$ and $n_i = 4$, the P_f(s) are 0.15 and 0.055 for Uniform prior, and 0.13 and 0.02 for Normal prior, respectively. As per USACE ETL-1110-2-547 (USACE 1997), this performance level corresponds to *Poor* to *Hazardous*, which clearly emphasizes the efficacy of the probabilistic approach towards a more realistic reliability assessment of the considered MLCS.
- Deterministic analysis for 30% slope points out the interface $n_i = 1$ to be safe (FoS ≥1.5) for 30 m length of the slope (Yamsani et al. 2019); however, simulation results considering normal priors show that P_f for these two interfaces is as high as 0.5-0.7.
- For the movement of a downward compacting vehicle, deterministic study concludes the interface $n_i = 1$ to be safe (FoS ≥1.5) for V=0 m (Yamsani et al. 2019). In contrast, the current probabilistic framework considering normal priors shows that the $n_i = 1$ interface has a mean FoS <1.5 and $P_f = 0.717$, which pertains to a hazardous performance level of the considered MLCS as per as per USACE ETL-1110-2-547 (USACE 1997).
- Considering all the destabilizing conditions, a probabilistic vulnerable interface diagram

(PVID) is developed for an anticipated worst-case scenario for the considered MLCS. The deterministic VID (Yamsani et al. 2019) considers both $n_i = 3$ and 5 to be safe, but the currently developed probabilistic vulnerability interface diagram (PVID) suggests that a fraction of FoS for $n_i = 3$ also do not satisfy the stability criterion. PVID suggests that interfaces $n_i = 1, 2$ and $n_i = 4$ are the most vulnerable ones. In a nutshell, except for the bottom-most interface, all the other interfaces of the considered MLCS are susceptible to critical failure and would require necessary strength improvement.

DATA AVAILABILITY STATEMENT

All data, models, or code that support the findings of this study are available from the corresponding author upon reasonable request.

ACKNOWLEDGMENTS

Budhaditya Hazra gratefully acknowledge the financial support received from Science and Engineering Research Board (SERB), Department of Science and Technology (DST), Government of India, (Project no. IMP/2019/000276).

REFERENCES

ASTM (2011). "Standard test method for direct shear test of soils under consolidated drained conditions." *ASTM D3080/3080M*, ASTM, West Conshohocken, PA.

Ching, J. and Phoon, K. K. (2019). "Constructing site-specific multivariate probability distribution model using bayesian machine learning." *Journal of Engineering Mechanics*, 145(1), 04018126.

Choudhury, D., Rajesh, B. G., and Savoikar, P. (2017). "Recent advances in seismic design of msw landfill considering stability." *Geoenvironmental practices and sustainability*, 31–37. Singapore: Springer.

Coulomb, C. (1776). "Essai sur une application des regles de maximis et minimis quelques problemes de statique, relatits a l'architecture." *Memoires de Mathematique de l'Academie Royale de Science, 7, Paris*.

EIA (2014). "Monthly energy review." *Energy Information Administration, US*.

El-Ramly, H., Morgenstern, N. R., and Cruden, D. M. (2002). "Probabilistic slope stability analysis for practice." *Canadian Geotechnical Journal*, 39(3), 665–683.

Fellin, W. and Oberguggenberger, M. (2012). "Robust assessment of shear parameters from direct shear tests." *International Journal of Reliability and Safety*, 6(1-3), 49–64.

Filliben, J. J. (1975). "The probability plot correlation coefficient test for normality." *Technometrics*, 17(1), 111–117.

Gelman, A., Carlin, J. B., Stern, H. S., Dunson, D. B., Vehtari, A., and Rubin, D. B. (2013). *Bayesian data analysis*. CRC press.

Geman, S. and Geman, D. (1984). "Stochastic relaxation, gibbs distributions, and the bayesian restoration of images." *IEEE Transactions on pattern analysis and machine intelligence*, 6, 721–741.

Griffiths, D. and Fenton, G. A. (2004). "Probabilistic slope stability analysis by finite elements." *Journal of geotechnical and geoenvironmental engineering*, 130(5), 507–518.

Hoffman, M. D. and Gelman, A. (2014). "The no-u-turn sampler: adaptively setting path lengths in hamiltonian monte carlo." *J. Mach. Learn. Res*, 15(1), 1593–1623.

Koerner, R. M. and Daniel, D. E. (1997). *Final covers for solid waste landfills and abandoned dumps*. American Society of Civil Engineers, Reston, VA.

Koerner, R. M. and Hwu, B. L. (1991). "Stability and tension considerations regarding cover soils on geomembrane lined slopes." *Geotextiles and Geomembranes*, 10(4), 335–355.

Koerner, R. M. and Soong, T. Y. (2005). "Analysis and design of veneer cover soils." *Geosynthetics International*, 12(1), 28–49.

Labuz, J. F. and Zang, A. (2012). "Mohr–coulomb failure criterion." *Rock Mechanics and Rock Engineering*, 45(6), 975–979.

Ling, H. I. and Leschinsky, D. (1997). "Seismic stability and permanent displacement of landfill cover systems." *Journal of Geotechnical and Geoenvironmental Engineering*, 123(2), 113–122.

Metropolis, N., Rosenbluth, A. W., Rosenbluth, M. N., Teller, A. H., and Teller, E. (1953). "Equation of state calculations by fast computing machines." *The journal of chemical physics*, 21(6), 1087–1092.

Mitchell, J. K., Seed, R. B., and Seed, H. B. (1990). "Kettleman hills waste landfill slope failure. i: Liner-system properties." *Journal of geotechnical engineering*, 116(4), 647–668.

Neal, R. M. (1993). *Probabilistic inference using Markov chain Monte Carlo methods*. Department of Computer Science, University of Toronto Toronto, ON, Canada.

Neal, R. M. et al. (2011). *MCMC using Hamiltonian dynamics. Handbook of markov chain monte carlo*. CRC press.

Nguyen, V. (1985). "Reliability index in geotechnics." *Computers and Geotechnics*, 1(2), 117–138.

Nishio, M. and Arakawa, A. (2019). "Performance of hamiltonian monte carlo and no-u-turn sampler for estimating genetic parameters and breeding values." *Genetics Selection Evolution*, 51(1), 1–12.

NSWEPA (2015). "Draft environmental guidelines solid waste landfills." *Online*, <https://www.epa.nsw.gov.au/>.

Prakash, A., Hazra, B., and Sreedeep, S. (2021). "Probabilistic analysis of soil-water characteristic curve using limited data." *Applied Mathematical Modelling*, 89, 752–770.

Seed, R. B., Mitchell, J. K., and Seed, H. B. (1990). "Kettleman hills waste landfill slope failure. ii: Stability analyses." *Journal of Geotechnical Engineering*, 116(4), 669–690.

Soubra, A. H. and Mao, N. (2012). "Probabilistic analysis of obliquely loaded strip foundations." *Soils and foundations*, 52(3), 524–538.

Soujanya, D. and Basha, B. M. (2023a). "Effect of hydrostatic and hydrodynamic pressures on the stability of landfill veneer covers with an internal sleeper." *ASCE-Journal of Hazardous, Toxic, and Radioactive Waste*, ASCE, 27(3), 04023013–1–14.

Soujanya, D. and Basha, B. M. (2023b). "Probabilistic stability analysis of reinforced veneer cover systems of msw landfills using monte carlo simulations." *Indian Geotechnical Journal*.

USACE (1997). "Engineering and design: Introduction to probability and reliability methods for use in geotechnical engineering." *Engineer Technical Letter 1110-2-547*, Department of the Army, Washington DC, USA.

Wang, Y. and Akeju, O. V. (2016). "Quantifying the cross-correlation between effective cohesion and friction angle of soil from limited site-specific data." *Soils and Foundations*, 56(6), 1055–1070.

Wang, Y., Zhao, T., and Cao, Z. (2015). "Site-specific probability distribution of geotechnical properties." *Computers and Geotechnics*, 70, 159–168.

Williams, M. N., Grajales, C. A. G., and Kurkiewicz, D. (2013). "Assumptions of multiple regression: Correcting two misconceptions." *Practical Assessment, Research and Evaluation*, 18(11).

Xu, X., Zhou, X., Huang, X., and Xu, L. (2017). "Wedge-failure analysis of the seismic slope using the pseudodynamic method." *International Journal of Geomechanics*, 17(12), 04017108.

Yamsani, S., Sreedeep, S., and Rakesh, R. R. (2016). "Frictional and interface frictional characteristics of multi-layer cover system materials and its impact on overall stability." *International Journal of Geosynthetics and Ground Engineering*, 2(3), 1–9.

Yamsani, S. K., Dey, A., Sekharan, S., and Rakesh, R. R. (2019). "Vulnerable interface diagram for translational stability analysis of multilayered cover system." *International Journal of*

Geomechanics, 19(12), 04019130.

List of Tables

TABLE 1. Shear strength parameters of considered geomaterials

Material types	**Cohesion**	**Angle of internal friction** ϕ (°)
Red soil (R)	16.96	14.2
Bentonite (B)	14.34	6.2
Gravel (G)	0	29.5
Sand (S)	0	26.9

TABLE 2. Details of different interfaces in MLCS

Interface n_i	**Upper component**	**Unit weight,** γ **(kN/m**^{3}**)**	**Lower component**	**Interface friction angle,** δ (°)	**Interfacial adhesion,** c **(kPa)**
1	Red soil	16.68	Geotextile	11.7	13.7
2	Geotextile	6.5	Gravel	9.1	0
3	Gravel	13.16	Sand	22.1	0
4	Sand	14.58	Geomembrane	16.7	0
5	Geomembrane	2.20	Bentonite	19.6	29.4

TABLE 3. Parameters of the uniform and normal priors

Interface	Uniform priors		Normal priors			
	c	v	μ_c	σ_c	μ_v	σ_v
Red soil-Geotextile (R-GT)	[4, 16]	[0.17, 0.24]	10	2	0.207	0.011
Geotextile-Gravel (GT-G)	-	[0.03, 0.3]	-	-	0.163	0.045
Gravel-Sand (G-S)	-	[0.32, 0.49]	-	-	0.409	0.029
Sand-Geomembrane (S-GM)	-	[0.14, 0.48]	-	-	0.308	0.058
Geomembrane-Bentonite (GM-B)	[6, 28.5]	[0.21, 0.51]	17.25	3.75	0.363	0.05

TABLE 4. R^2 obtained from probability plots

Interface	Candidate Distribution	Noninformative priors $c(\mathbf{R}^2)$	Noninformative priors $v(\mathbf{R}^2)$	Informative priors $c(\mathbf{R}^2)$	Informative priors $v(\mathbf{R}^2)$
Redsoil-Geotextile	Weibull	**0.982**	**0.959**	0.988	0.964
	Normal	0.958	0.957	**0.999**	**0.999**
	Lognormal	0.866	0.939	0.985	0.998
	Gumbel	0.815	0.836	0.938	0.936
Geotextile-Gravel	Weibull	-	0.979	-	0.977
	Normal	-	**0.999**	-	**0.999**
	Lognormal	-	0.993	-	0.995
	Gumbel	-	0.941	-	0.941
Gravel-Sand	Weibull	-	0.944	-	0.965
	Normal	-	**0.974**	-	**0.999**
	Lognormal	-	0.969	-	0.998
	Gumbel	-	0.906	-	0.942
Sand-Geomembrane	Weibull	-	0.986	-	0.973
	Normal	-	**0.999**	-	**0.999**
	Lognormal	-	0.988	-	0.996
	Gumbel	-	0.942	-	0.942
Geomembrane-Bentonite	Weibull	**0.972**	**0.989**	0.989	0.973
	Normal	0.954	0.975	**0.999**	**0.999**
	Lognormal	0.829	0.941	0.985	0.996
	Gumbel	0.813	0.851	0.943	0.942

TABLE 5. R^2 obtained from probability plots of FoS

Interface	**Candidate Distribution**	**FoS (R^2) (Posteriors from noninformative priors)**			**FoS (R^2) (Posteriors from informative priors)**		
		β **= 5.7**°	β **= 11.3**°	β **= 16.7**°	β **= 5.7**°	β **= 11.3**°	β **= 16.7**°
Redsoil-Geotextile	Weibull	0.997	0.989	0.988	0.999	0.999	0.999
	Normal	**0.998**	**0.998**	**0.998**	**0.999**	**0.999**	**0.999**
	Lognormal	0.992	0.993	0.993	0.998	0.997	0.997
	Gumbel	0.913	0.924	0.924	0.934	0.933	0.933
Geotextile-Gravel	Weibull	0.989	0.983	0.981	0.999	0.998	0.998
	Normal	**0.999**	**0.999**	**0.999**	**0.999**	**0.999**	**0.999**
	Lognormal	0.998	0.997	0.997	0.999	0.998	0.998
	Gumbel	0.941	0.941	0.942	0.942	0.943	0.944
Gravel-Sand	Weibull	0.963	0.953	0.952	0.998	0.998	0.998
	Normal	**0.974**	**0.974**	**0.974**	**0.999**	**0.999**	**0.999**
	Lognormal	0.973	0.972	0.972	0.999	0.998	0.998
	Gumbel	0.906	0.906	0.906	0.942	0.942	0.942
Sand-Geomembrane	Weibull	0.989	0.983	0.981	0.998	0.998	0.998
	Normal	**0.999**	**0.999**	**0.999**	**0.999**	**0.999**	**0.999**
	Lognormal	0.998	0.997	0.997	0.999	0.999	0.999
	Gumbel	0.942	0.943	0.944	0.946	0.946	0.947
Geomembrane-Bentonite	Weibull	**0.999**	**0.998**	**0.998**	0.998	0.998	0.998
	Normal	0.989	0.982	0.981	**0.999**	**0.999**	**0.999**
	Lognormal	0.980	0.968	0.966	0.999	0.999	0.999
	Gumbel	0.882	0.864	0.862	0.945	0.944	0.944

TABLE 6. P_f, Mean FoS, 95^{th}, and 99^{th} percentile FoS (noninformative priors) for varying inclination of MLCS (30 m length of slope)

Inclination of MLCS	Interface	Yamsani et al 2019	Bayesian Linear Regression			
		FOS	Mean FOS	95% quantile	99% quantile	P_f
$tan\beta$ **= 10%**	R-GT	6.74	6.62	7.01	7.14	0
	GT-G	4.66	4.67	4.98	5.10	0
	G-S	6.22	6.19	6.93	7.03	0
	S-GM	5.07	5.05	5.79	6.12	0
	GM-B	8.27	8.49	9.16	9.17	0
$tan\beta$ **= 20%**	R-GT	2.43	2.39	2.55	2.61	0
	GT-G	1.62	1.59	1.75	1.81	0.15
	G-S	2.45	2.39	2.76	2.82	0
	S-GM	1.901	1.86	2.22	2.39	0.055
	GM-B	3.15	3.28	3.61	3.70	0
$tan\beta$ **= 30%**	R-GT	1.52	1.49	1.603	1.64	**0.5055**
	GT-G	1.008	1.01	1.11	1.15	**1**
	G-S	1.55	1.54	1.78	1.82	0.4201
	S-GM	1.19	1.19	1.425	1.54	**0.9811**
	GM-B	1.99	2.11	2.33	2.39	0

TABLE 7. P_f, Mean FoS, 95^{th}, and 99^{th} percentile FoS (informative priors) for varying inclination of MLCS (30 m length of slope)

Inclination of MLCS	Interface	Yamsani et al 2019	Bayesian Linear Regression			
		FOS	Mean FOS	95% quantile	99% quantile	P_f
$tan\beta$ = **10%**	R-GT	6.74	6.51	6.8	6.94	0
	GT-G	4.66	4.67	4.95	5.07	0
	G-S	6.22	6.24	6.68	6.84	0
	S-GM	5.07	5.08	5.68	5.94	0
	GM-B	8.27	8.27	8.85	9.11	0
$tan\beta$ = **20%**	R-GT	2.43	2.35	2.46	2.52	0
	GT-G	1.62	1.59	1.74	1.8	0.1305
	G-S	2.45	2.42	2.64	2.72	0
	S-GM	1.901	1.87	2.17	2.3	0.0188
	GM-B	3.15	3.17	3.46	3.59	0
$tan\beta$ = **30%**	R-GT	1.52	1.47	1.55	1.58	**0.7174**
	GT-G	1.008	1.01	1.103	1.14	**1**
	G-S	1.55	1.55	1.69	1.75	0.2818
	S-GM	1.19	1.19	1.39	1.48	**0.9939**
	GM-B	1.99	2.04	2.23	2.31	0

TABLE 8. P_f, Mean FoS, 95^{th}, and 99^{th} percentile FoS (informative priors) for varying lengths of MLCS (30% slope)

Length of MLCS	Interface	Yamsani et al 2019	Bayesian Linear Regression			
		FOS	**Mean** FOS	**95% quantile**	**99% quantile**	P_f
L = 15 m	R-GT	2.72	2.59	2.73	2.79	0
	GT-G	1.67	1.68	1.77	1.81	0
	G-S	1.82	1.83	1.97	2.03	0
	S-GM	1.46	1.46	1.66	1.75	**0.629**
	GM-B	3.15	3.05	3.25	3.34	0
L = 30 m	R-GT	1.52	1.47	1.55	1.57	**0.717**
	GT-G	1.0	1.01	1.1	1.14	**1**
	G-S	1.55	1.55	1.69	1.76	0.281
	S-GM	1.19	1.19	1.39	1.48	**0.993**
	GM-B	2.0	2.04	2.23	2.31	0
L = 50 m	R-GT	1.16	1.14	1.19	1.22	**1**
	GT-G	0.8	0.81	0.89	0.93	**1**
	G-S	1.5	1.47	1.61	1.67	**0.642**
	S-GM	1.11	1.11	1.31	1.4	**0.999**
	GM-B	1.64	1.73	1.93	2.01	0.027

List of Figures

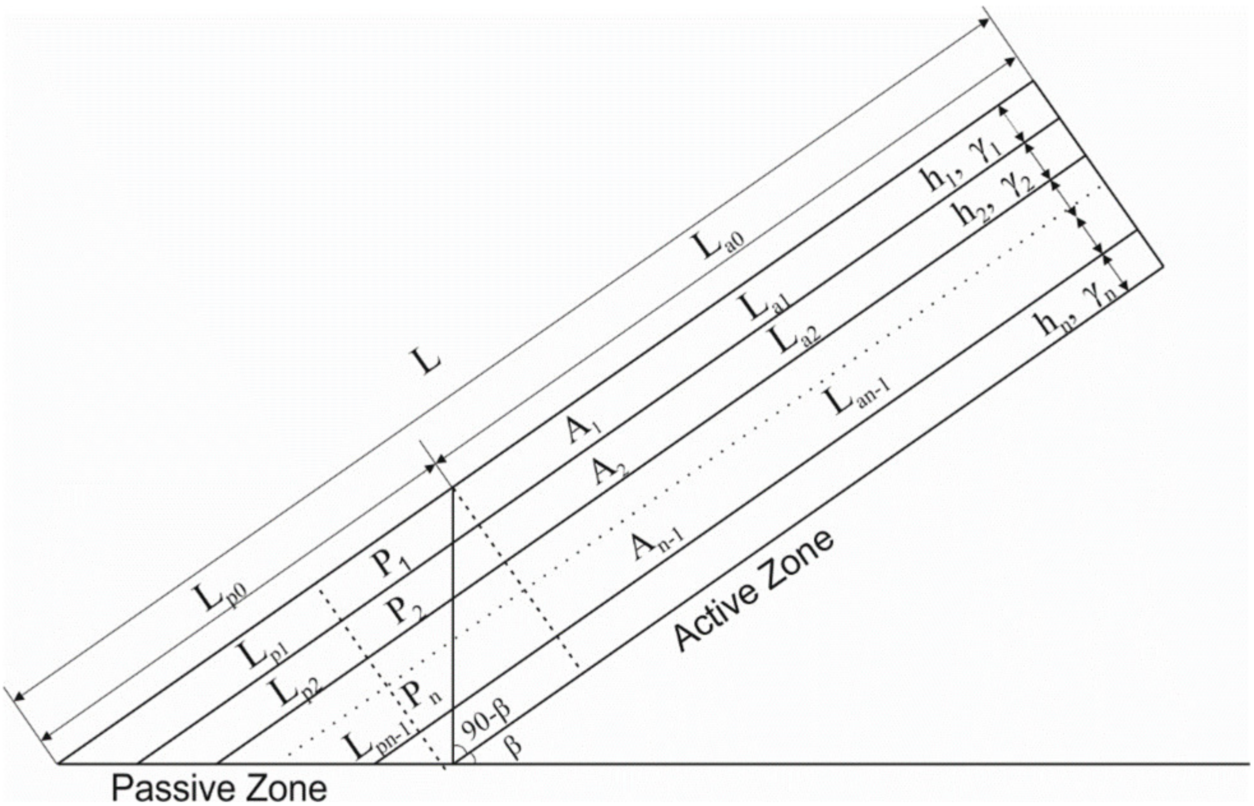

Fig. 1. Schematic of MLCS.

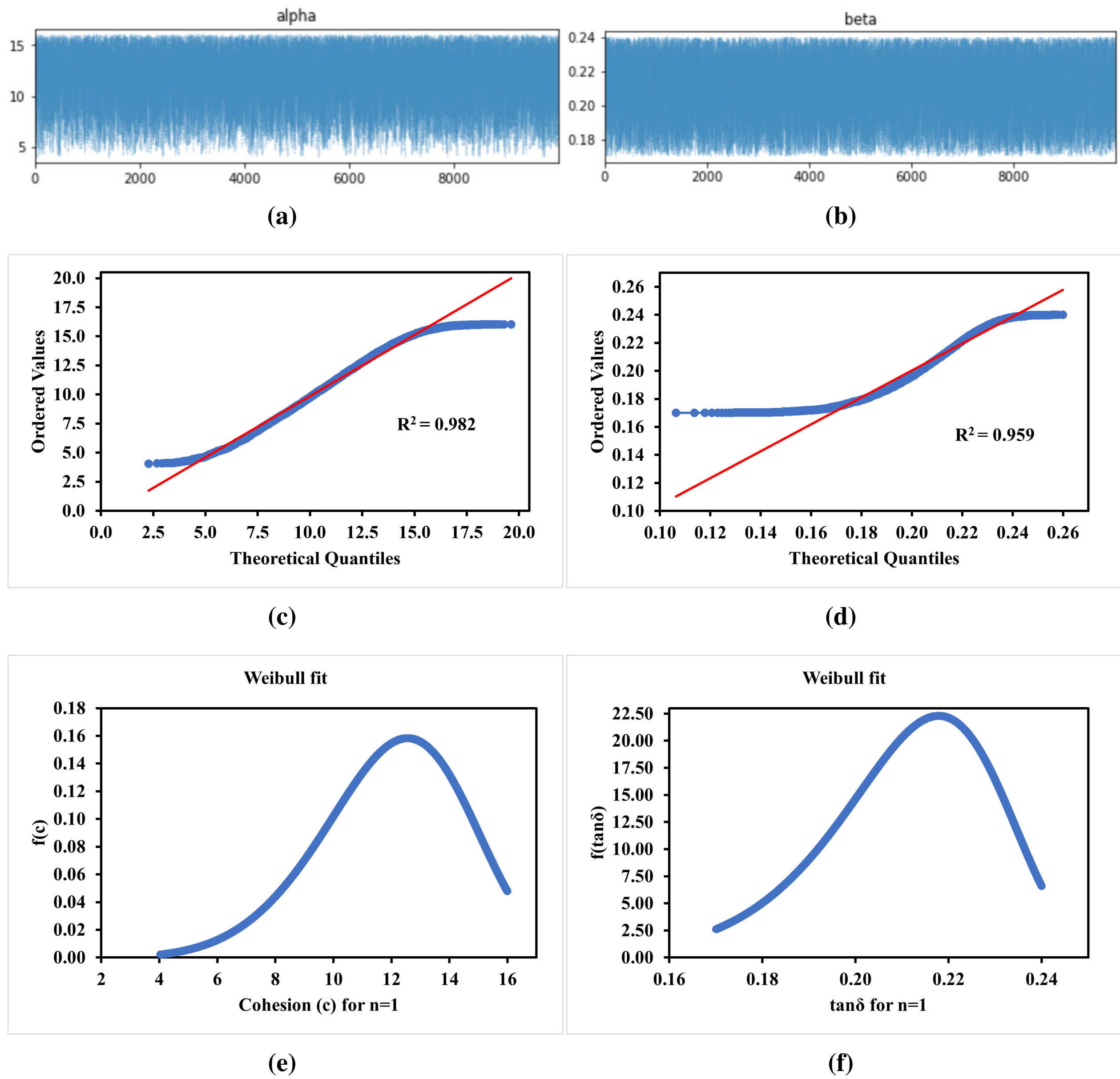

Fig. 2. Trace plots of red soil-geotextile interface (n = 1) characteristics (a) c, (b) v along the length of MCMC chain along with best-fit probability plots of posteriors for (c) c, (d) v, and marginal density plots of posteriors for (e) c, (f) v considering uniform priors.

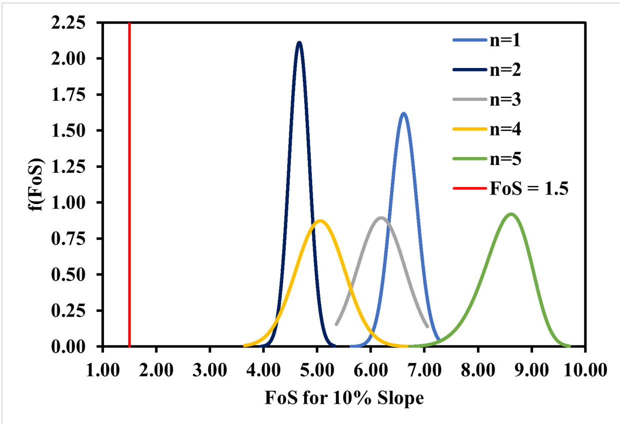

(a)

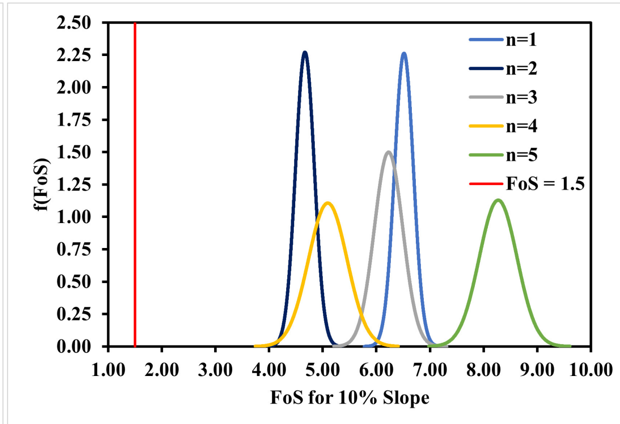

(b)

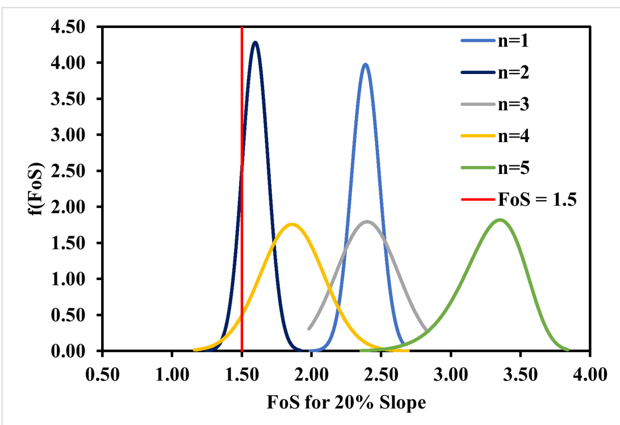

(c)

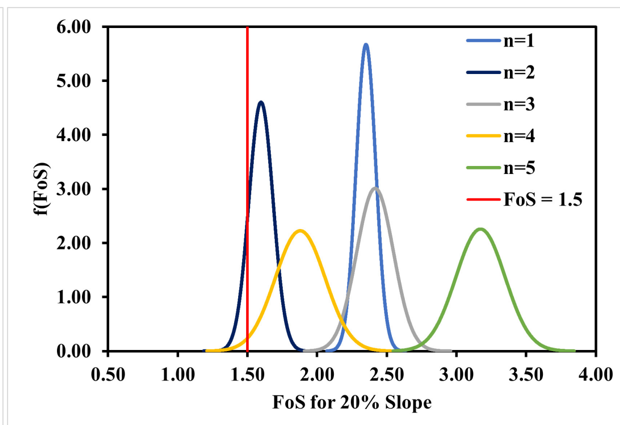

(d)

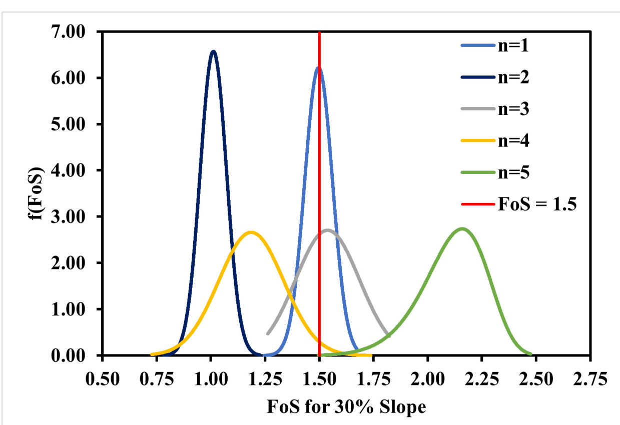

(e)

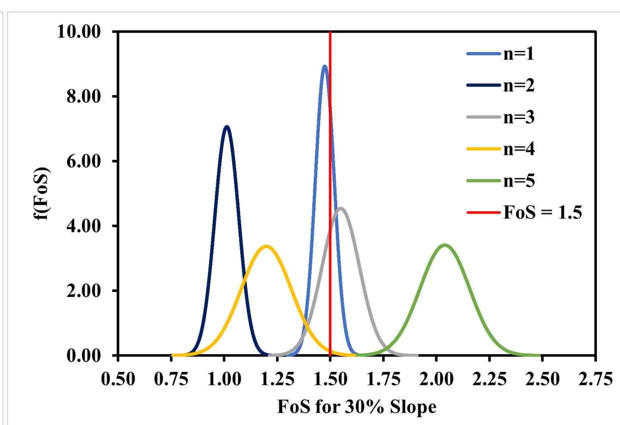

(f)

Fig. 3. FoS distribution for interfaces (n = 1 to 5) after sampling posteriors obtained from MCMC: when priors are uniform considering (a) 10% (c) 20% (e) 30% slope inclination; when priors are normal considering (b) 10% (d) 20% (f) 30% slope inclination for L = 30 m.

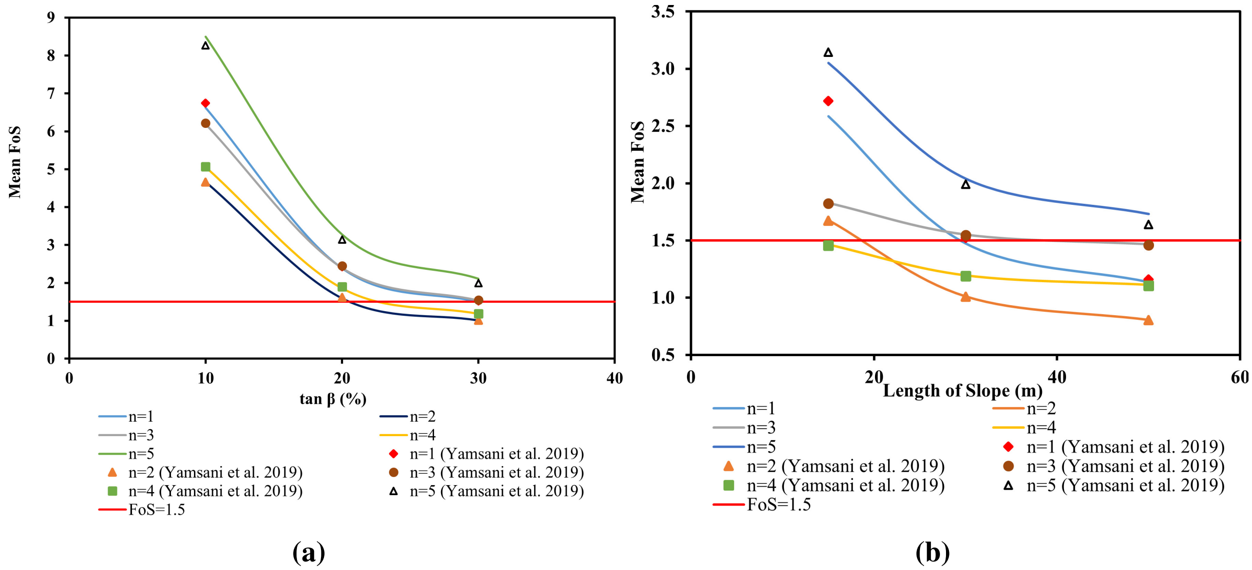

Fig. 4. Mean FoS of MLCS with change in (a) slope after sampling posteriors from MCMC when priors are uniform (b) length after sampling posteriors from MCMC when priors are normal.

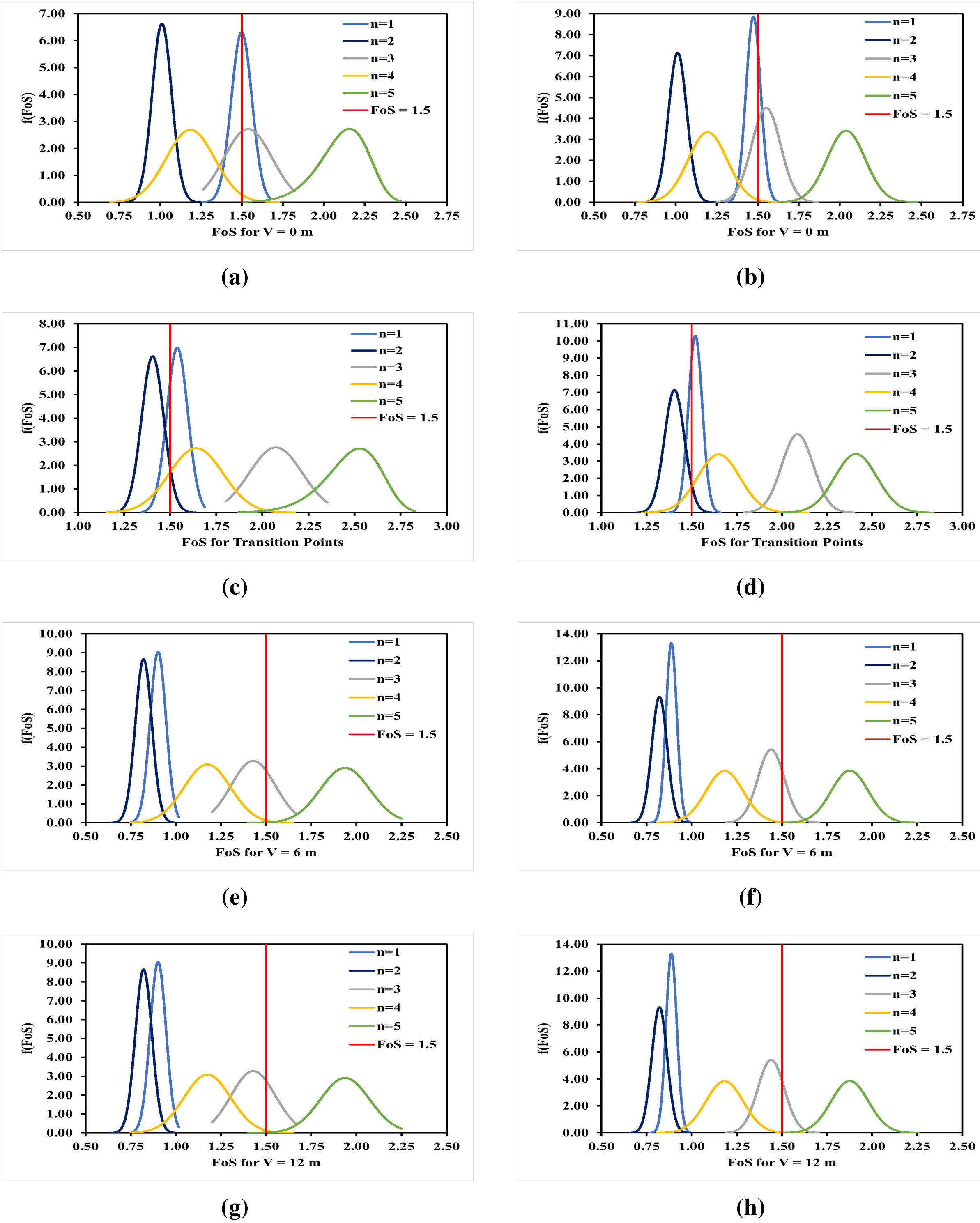

Fig. 5. FoS distribution for interfaces (n = 1 to 5) after sampling posteriors obtained from MCMC: when priors are uniform considering V (a) 0 m (c) Transition point (e) 6 m (g) 12 m.; when priors are normal considering V (b) 0 m (d) Transition point (f) 6 m (h) 12 m.

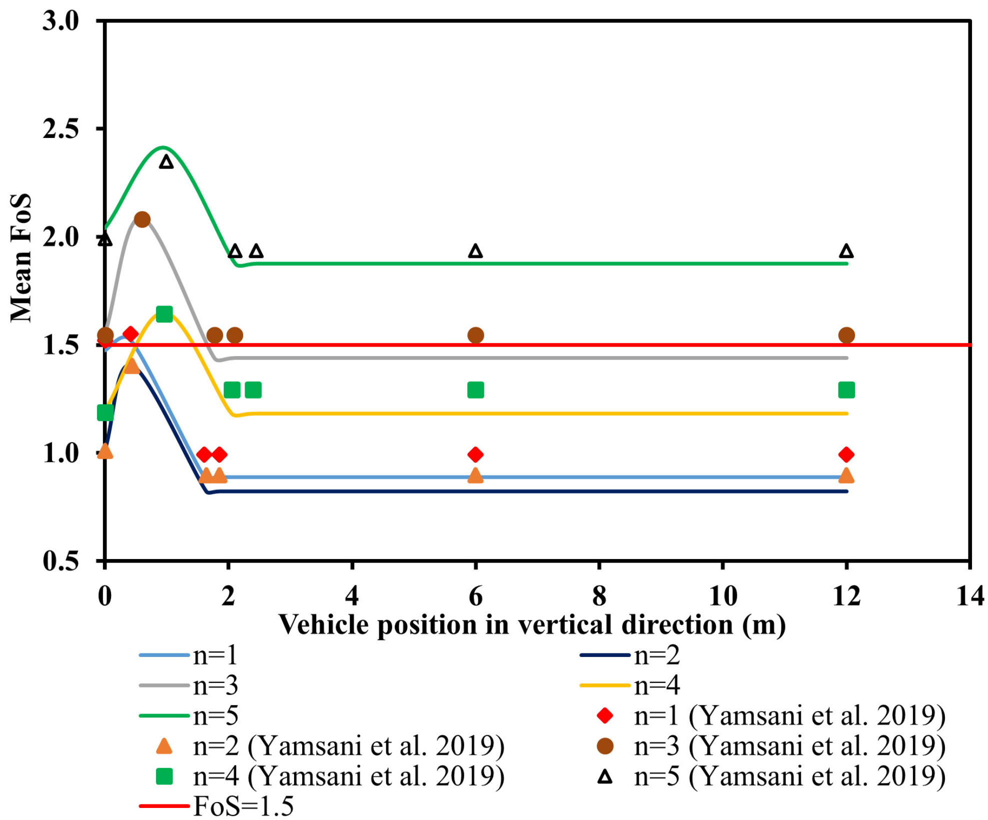

Fig. 6. Mean FoS of MLCS with change in vertical position of vehicle descending the slope after sampling posteriors from MCMC when priors are normal.

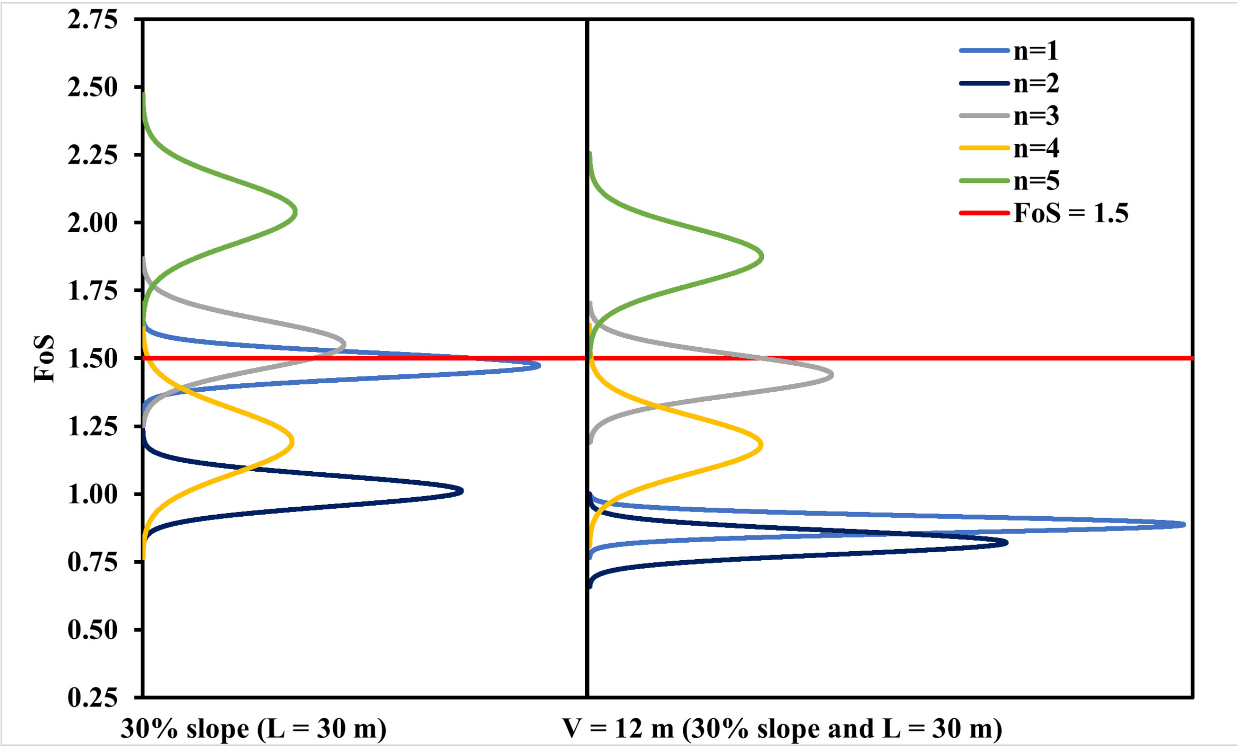

Fig. 7. Probabilistic vulnerable interface diagram for MLCS considering Normal priors.

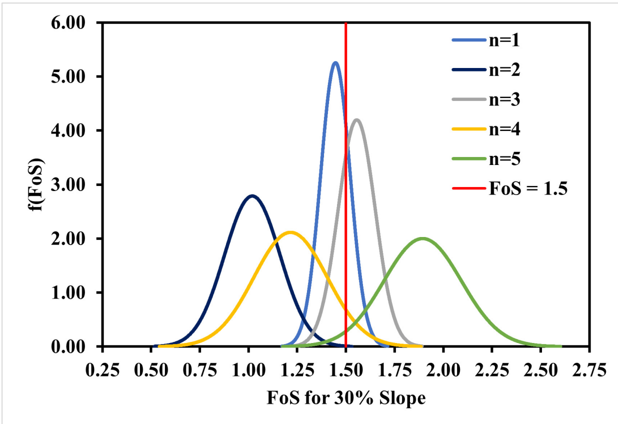

(a)

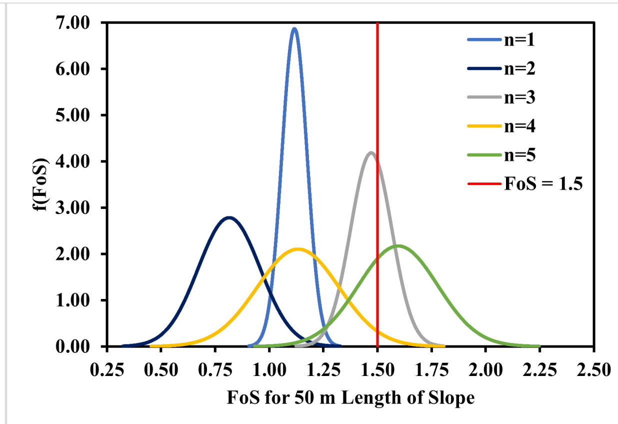

(b)

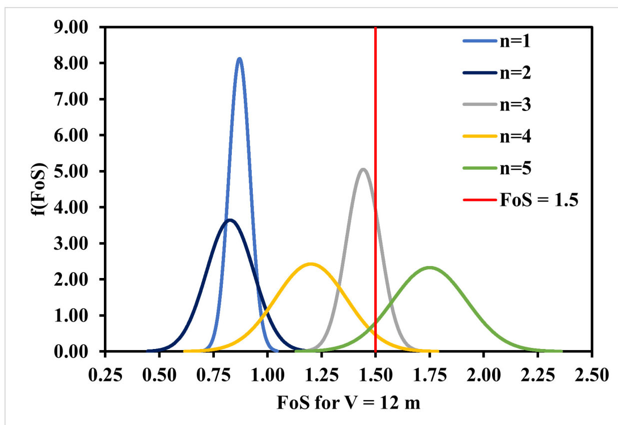

(c)

Fig. 8. FoS distribution for interfaces (n = 1 to 5) after sampling *c*, *v* directly from the normal distribution considering (a) 30% slope (b) 50 m length of slope and (c) V = 12m.